A Monotone Streamline Upwind Finite Element Method for 6-nodes Triangular Elements

Niphon Wansophark[a,*] and Pramote Dechaumphai[a]
[a]Department of Mechanical Engineering, Chulalongkorn University

Abstract

A scheme of streamline upwind finite element method using the 6-nodes triangular element is presented. The method is applied to the convection term of the governing transport equation directly along the local streamlines. Several examples are selected and used to evaluate the method. Results show that the scheme is monotonic and does not produce any oscillation. In addition, an adaptive meshing technique is combined with the method to further increase the solution accuracy, and at the same time, to minimize the computational time and computer memory requirement.

Keywords: Streamline Upwind, Finite Element Method.

1. Introduction

Accurate numerical solution of the convection dominated flow problem is one of the difficult tasks to achieve. Central difference method and the conventional Galerkin method have consistently yield unphysical oscillatory solutions. One successful technique for solving such problem is known as the upwind algorithm which originally devised for finite difference method [1]. In finite element method, the widely used technique is known as Streamline Upwind Petrov-Galerkin (SUPG) method [2]. This method modifies the weighting functions by using the local velocity to dictate an upstream direction of these functions. Such modification eliminates the oscillatory behavior on some convection problems. Another successful method is the Streamline Upwinding Finite Element Method, which originally proposed by Rice and Schnipke [3]. The method evaluates convection terms directly along the local streamlines on the 4-nodes bi-linear element instead of modifying the weighting functions. Calculations presented in their paper have shown that the method is monotonic and introduces artificial numerical diffusion. The effect of numerical diffusion is to smear the solution in area of high flow field gradients and hence decreases the solution accuracy.

The accuracy in a numerical solution is an important factor that must be considered especially for large size problems. The solution accuracy can be increased by using small elements in the computational domain, but it will require additional computer time and data storage [4]. To reduce such difficulties, a technique of adaptive meshing [5] is incorporated in the computational algorithm.

In this paper, the procedure to compute the convection terms along local streamlines passing through the 6-nodes triangular elements is presented. The triangular elements are employed in order to combine effectively with the adaptive meshing technique presented herein. Finally, the finite element formulation and the computer program have been verified using several examples that have prior numerical solutions.

2. Theoretical Formulation and Solution Procedure

In this section, the transport equation is selected as a typical equation for convective-diffusion problem. Typical two-dimensional transport equation in the Cartesian coordinates is,

$$\rho\left(u\frac{\partial\phi}{\partial x}+v\frac{\partial\phi}{\partial y}\right)=\Gamma_\phi\left(\frac{\partial^2\phi}{\partial x^2}+\frac{\partial^2\phi}{\partial y^2}\right) \qquad (1)$$

where ρ is the density, u and v are the velocity components in x and y direction, Γ_ϕ is the

diffusivity coefficient and ϕ is the quantity being transported in the flow field.

2.1 Finite Element Algorithm

To derive the finite element equations, the 6-nodes triangular element as illustrated in Fig. 1 is used in this study. The Galerkin's method of weighted residuals is applied to the governing equation (1) with the standard weighting function, N. The element equations are,

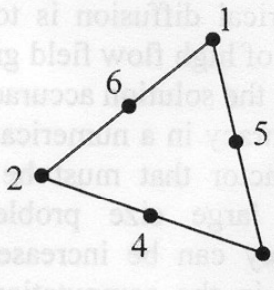

Fig. 1. The 6-nodes triangular elements.

$$\rho \int_{\Omega} N\left(u\frac{\partial \phi}{\partial x}+v\frac{\partial \phi}{\partial y}\right)d\Omega = \Gamma_{\phi}\int_{\Omega}\left(\frac{\partial N}{\partial x}\frac{\partial \phi}{\partial x}+\frac{\partial N}{\partial y}\frac{\partial \phi}{\partial y}\right)d\Omega \quad (2)$$

where Ω is the element area. Then, the diffusion terms on the right-hand side of (2) are treated by performing integration by parts using the Gauss theorem [6]. The special treatment for the convection term is discussed in the following section.

2.2 Streamline Upwind Formulation

The concept of the streamline upwind formulation for convection terms is best described by considering a pure convection problem with no physical diffusion. In this case, the Galerkin's method of weighted residuals yields,

$$\int_{\Omega} N\left(\rho u\frac{\partial \phi}{\partial x}+\rho v\frac{\partial \phi}{\partial y}\right)d\Omega = 0 \quad (3)$$

With the streamline coordinates as shown in Fig. 2, Eq. (3) can be rewritten as,

$$\int_{\Omega} N\left(\rho U_S\frac{\partial \phi}{\partial s}\right)d\Omega = 0 \quad (4)$$

where U_S is the velocity in the streamline direction. On an element it is assumed that [3],

$$\rho U_S\frac{\partial \phi}{\partial s} = \text{constant} \quad (5)$$

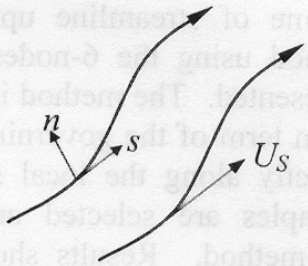

Fig. 2. Streamline coordinates.

Then, the element convection term is approximated as,

$$\left(\rho U_S\frac{\partial \phi}{\partial s}\right)\int_{\Omega} N\,d\Omega = 0 \quad (6)$$

The evaluation of Eq. (6) requires the location of an upwind point every time a downwind point is detected. In Figure 3, node 1 on this element is called the "downwind node" because the negative of the velocity vector at this node points back into the element. In the case of corner nodes, the method for finding the downwind node is straightforward and can be expressed mathematically as,

$$\tan\alpha \le \tan\theta \le \tan\beta \quad (7)$$

The condition of Eq. (7) must be satisfied on any downwind node.

For the mid-side nodes, Fig. 4 shows the condition that must be used to detect the downwind node and can be written by the following expression,

$$\vec{V}\cdot\hat{n} \ge 0 \quad (8)$$

where $\vec{V}$ is the velocity vector at mid-side node and $\hat{n}$ is the normal vector on that side of the element.

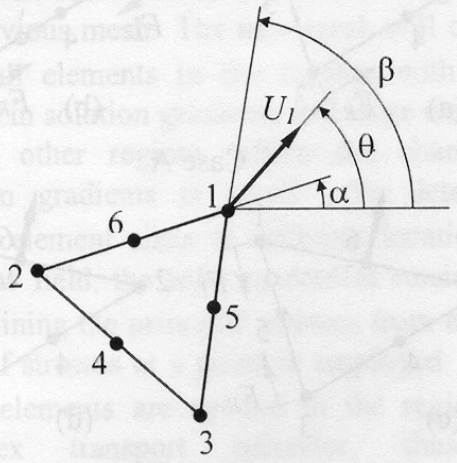

Fig. 3. Downwind node detection for a corner node.

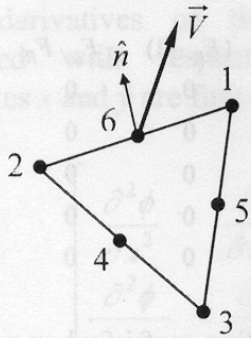

Fig. 4. Downwind node detection for a mid-side node.

Once a downwind node is detected, the mass flow rates at each side of the element as shown in Fig. 5 are calculated. The upwind point can be found from these mass flow rates. Figure 6 shows the possible cases that could occur when node 1 is the downwind node. In this figure, the location of the upwind point (x_U, y_U) can be determined by the factor F_L and F_R which are calculated from the ratio of mass flow rates on each side of the element and can be expressed as,

$$F_L = \max\left\{\min\left\{\frac{f3a+f3b}{f1a},1\right\},0\right\} \qquad (9)$$

$$F_R = \max\left\{\min\left\{\frac{f2a+f2b}{f1b},1\right\},0\right\} \qquad (10)$$

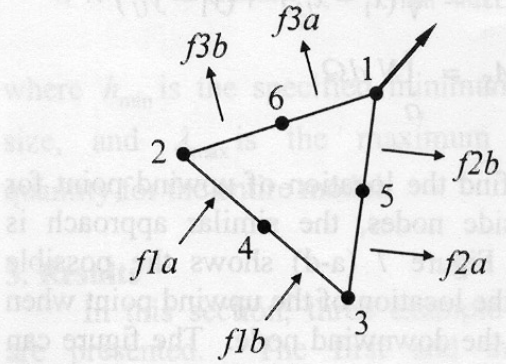

Fig. 5. Definition of mass flow rates.

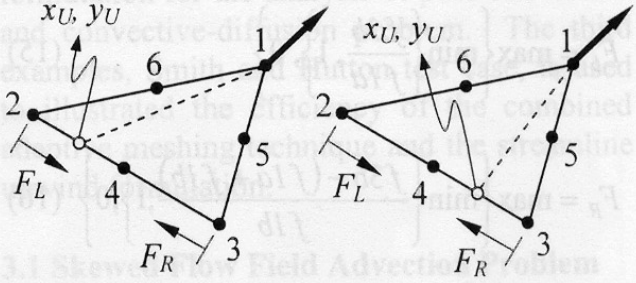

Fig. 6. Possible upwind points for corner nodes.

After that, the upwind point is calculated from,

$$x_U = (1-F_L)x_2 + (1-F_R)x_3 + (F_L \cdot F_R)x_4 \qquad (11)$$

$$y_U = (1-F_L)y_2 + (1-F_R)y_3 + (F_L \cdot F_R)y_4 \qquad (12)$$

Similarly, the quantity being transported at the upwind point, ϕ_U, is determined as,

$$\phi_U = (1-F_L)\phi_2 + (1-F_R)\phi_3 + (F_L \cdot F_R)\phi_4 \qquad (13)$$

Then the convection term in Eq. (6) when node 1 is downwind node can be evaluated from,

$$\left(\rho U_S \frac{\phi_1 - \phi_U}{\Delta s}\right) A_S = 0 \qquad (14)$$

where $U_S = \sqrt{u_1^2 + v_1^2}$

$$\Delta s = \sqrt{(x_1 - x_U)^2 + (y_1 - y_U)^2}$$

$$A_S = \int_{\Omega} N \, d\Omega$$

To find the location of upwind point for the mid-side nodes, the similar approach is applied. Figure 7 (a-d) shows the possible cases for the location of the upwind point when node 6 is the downwind node. The figure can be divided into 2 major cases, case A and B. For case A (Fig. 7(a-b)), it happens when *f3b < (f1a+f1b)* and the factor F_L and F_R can be calculated from,

$$F_L = \max\left\{\min\left\{\frac{f3b}{f1a}, 1\right\}, 0\right\} \quad (15)$$

$$F_R = \max\left\{\min\left\{\frac{f3b - (f1a + f1b)}{f1b}, 1\right\}, 0\right\} \quad (16)$$

The condition for case B (Fig. 7(c-d)) is *f3a < (f2a+f2b)*, the factor F_L and F_R are,

$$F_L = \max\left\{\min\left\{\frac{f3a}{f2b}, 1\right\}, 0\right\} \quad (17)$$

$$F_R = \max\left\{\min\left\{\frac{f3a - (f2a + f2b)}{f2a}, 1\right\}, 0\right\} \quad (18)$$

To find the location of the upwind point, the similar expression as given by Eq. (11-13) can be used.

The final step is to construct the element matrix for the convection term. Figure 8 shows the convection matrix when node 1, which is the corner node, is the only downwind node. For the mid-side node, such as node 6 in Fig. 7, the convection matrices for case A and B are shown in Fig. 9(a-b) respectively.

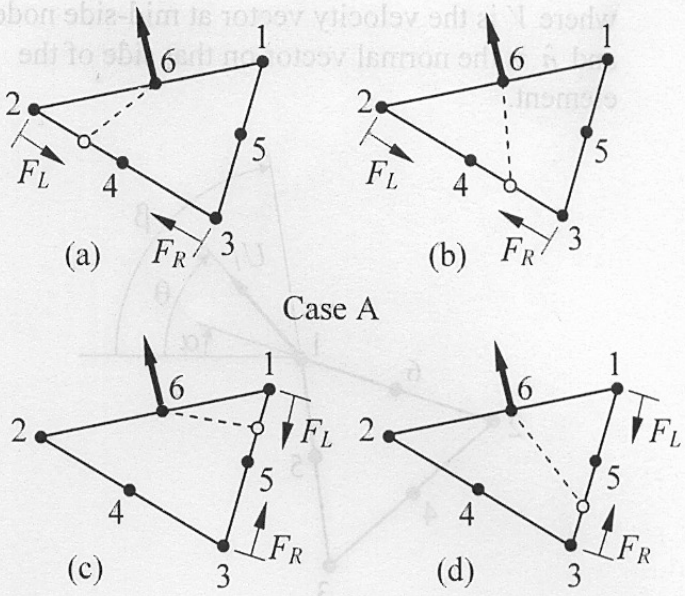

Fig. 7. Possible upwind points for mid-side nodes.

$$\rho U_S \frac{A_S}{\Delta s} \cdot \begin{bmatrix} 1 & (F_L - 1) & (F_R - 1) & -F_L \cdot F_R & 0 & 0 \\ 0 & 0 & 0 & 0 & 0 & 0 \\ 0 & 0 & 0 & 0 & 0 & 0 \\ 0 & 0 & 0 & 0 & 0 & 0 \\ 0 & 0 & 0 & 0 & 0 & 0 \\ 0 & 0 & 0 & 0 & 0 & 0 \end{bmatrix} \begin{Bmatrix} \phi_1 \\ \phi_2 \\ \phi_3 \\ \phi_4 \\ \phi_5 \\ \phi_6 \end{Bmatrix}$$

Fig. 8. Convection matrix when node 1 is the downwind node.

$$\rho U_S \frac{A_S}{\Delta s} \cdot \begin{bmatrix} 0 & 0 & 0 & 0 & 0 & 0 \\ 0 & 0 & 0 & 0 & 0 & 0 \\ 0 & 0 & 0 & 0 & 0 & 0 \\ 0 & 0 & 0 & 0 & 0 & 0 \\ 0 & 0 & 0 & 0 & 0 & 0 \\ 0 & (F_L - 1) & (F_R - 1) & -F_L \cdot F_R & 0 & 1 \end{bmatrix} \begin{Bmatrix} \phi_1 \\ \phi_2 \\ \phi_3 \\ \phi_4 \\ \phi_5 \\ \phi_6 \end{Bmatrix}$$

(a)

$$\rho U_S \frac{A_S}{\Delta s} \cdot \begin{bmatrix} 0 & 0 & 0 & 0 & 0 & 0 \\ 0 & 0 & 0 & 0 & 0 & 0 \\ 0 & 0 & 0 & 0 & 0 & 0 \\ 0 & 0 & 0 & 0 & 0 & 0 \\ 0 & 0 & 0 & 0 & 0 & 0 \\ (F_L - 1) & 0 & (F_R - 1) & 0 & -F_L \cdot F_R & 1 \end{bmatrix} \begin{Bmatrix} \phi_1 \\ \phi_2 \\ \phi_3 \\ \phi_4 \\ \phi_5 \\ \phi_6 \end{Bmatrix}$$

(b)

Fig. 9. (a) convection matrix for case A (b) convection matrix for case B

2.3 Adaptive Meshing Technique

The idea behind the adaptive meshing technique presented herein is to construct a new mesh based on the solution obtained from the previous mesh. The new mesh will consist of small elements in the regions with large change in solution gradients and large elements in the other regions where the change in solution gradients is small. To determine proper element sizes at different locations in the flow field, the solid-mechanics concept for determining the principal stresses from a given state of stresses at a point is employed. Since small elements are needed in the regions of complex transport behavior, thus the distribution of quantity being transported, ϕ, can be used as an indicator in the determination of proper element sizes.

To determine proper element sizes, the second derivatives of the quantity being transported with respect to the global coordinates x and y are first computed,

$$\begin{bmatrix} \frac{\partial^2\phi}{\partial x^2} & \frac{\partial^2\phi}{\partial x\partial y} \\ \frac{\partial^2\phi}{\partial x\partial y} & \frac{\partial^2\phi}{\partial y^2} \end{bmatrix} \tag{19}$$

The principal quantities in the principal directions X and Y where the cross derivatives vanish, are then determined,

$$\begin{bmatrix} \frac{\partial^2\phi}{\partial X^2} & 0 \\ 0 & \frac{\partial^2\phi}{\partial Y^2} \end{bmatrix} \tag{20}$$

The magnitude of the larger principal quantity is then selected,

$$\lambda = \max\left(\left|\frac{\partial^2\phi}{\partial X^2}\right|, \left|\frac{\partial^2\phi}{\partial Y^2}\right| \right) \tag{21}$$

This value is used to compute proper element size h at that locations from the conditions,

$$h^2\lambda = \text{constant} = h_{\min}^2\lambda_{\max} \tag{22}$$

where $h_{\min}$ is the specified minimum element size, and $\lambda_{\max}$ is the maximum principal quantity for the entire model.

3. Results

In this section, three example problems are presented. The first and the second examples, the skewed flow field advection problem and the thermal entry problem, respectively, are chosen to evaluate the performance of the streamline upwind formulation for the analysis of pure convection and convective-diffusion problem. The third examples, Smith and Hutton test case, is used to illustrated the efficiency of the combined adaptive meshing technique and the streamline upwind formulation.

3.1 Skewed Flow Field Advection Problem

The first example for evaluating the streamline upwind formulation is the skewed flow field advection problem. The problem is the pure convection transport and always used in several publications for evaluating the accuracy and stability of proposed method in treating the convection term. The computational domain is simply a square region as illustrated in Figure 10. The velocity field is taken as uniform over the entire domain at the angle of 60 degrees with respect to x-axis.

For the boundary conditions, the value of ϕ is assigned along the inflow sides of the computational domain as a step discontinuity. Along the left side of the domain ϕ is one and along the bottom side ϕ is also one for $0 \le x \le 0.2$ and zero for $0.2 < x \le 1$ as shown in Figure 10.

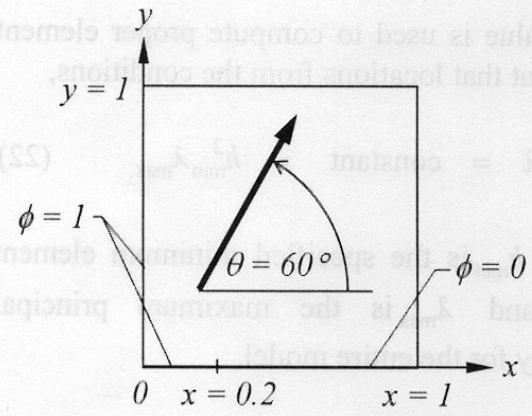

Fig. 10. Skewed flow field advection problem.

The results from the current method and the conventional approaches, such as standard Galerkin and Streamline Upwind Petrov-Galerkin (SUPG) method, are shown in Figures 11-12. As illustrated, the current method does not exhibit any non-physical oscillation.

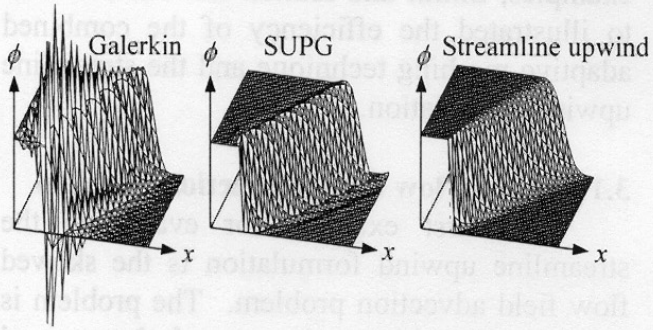

Fig. 11. Comparative results for skewed flow filed advection problem.

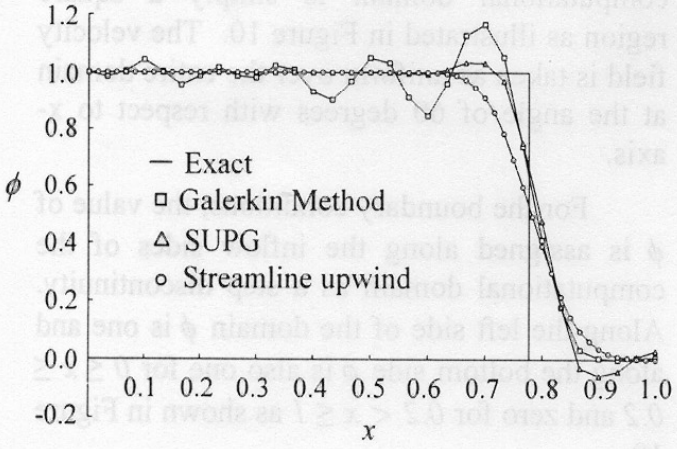

Fig. 12. Plots of numerical results along the outflow boundary from several methods.

3.2 Thermal Entry Problem

The second example is the thermal entry problem [7] where the cold fluid flows through a hot duct with a very high aspect ratio of the cross-section ($L >> a$) as shown in Fig. 13. Away from the side wall of the duct, the temperature distribution is effectively two-dimensional, thus the computational domain and the appropriate boundary conditions can be illustrated in Fig. 14.

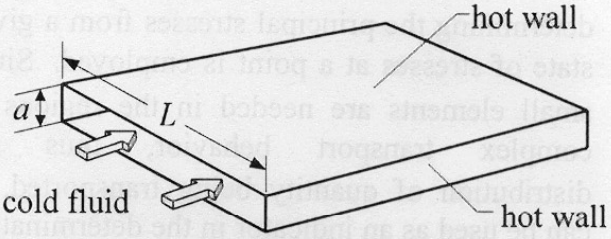

Fig. 13. Thermal Entry Problem.

For two-dimensional advective-diffusion problem, the governing equation as shown in Eq. (23) is used,

$$\rho u\frac{\partial T}{\partial x}+\rho v\frac{\partial T}{\partial y}=\Gamma_x\frac{\partial^2 T}{\partial x^2}+\Gamma_y\frac{\partial^2 T}{\partial y^2} \qquad (23)$$

where $\Gamma_x=\dfrac{10}{\mathrm{PrRe}^2}$, $\Gamma_y=\dfrac{1.6}{\mathrm{Pr}}$, Re and Pr are the Reynolds and Prandtl numbers, respectively.

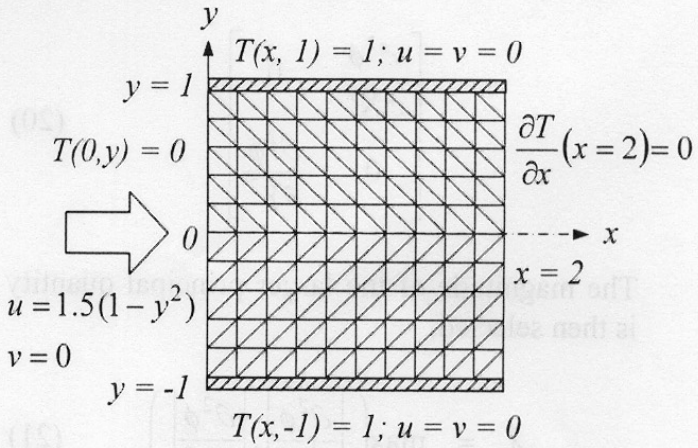

Fig. 14. Computational domain and boundary condition for thermal entry problem.

To compare the temperature distribution along the center of the duct with a semi-analytic solution [8], a fully developed velocity distribution is assigned over entire domain as $u = 1.5(1-y^2)$, $v = 0$ and the value of Pr and Re are 0.7 and 100, respectively. Figure 15 shows the comparison of the temperature distributions from presented algorithm along the center of the duct and the result from [8]. From the figure, the result from the current method follows the semi-analytic solution very well.

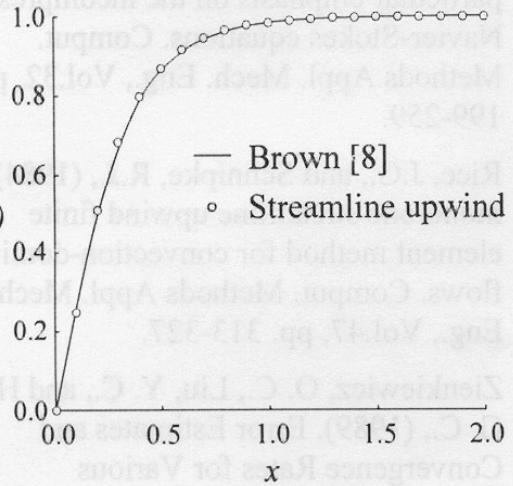

Fig. 15. Comparison of temperature distributions along center of computational domain.

3.3 Smith and Hutton Test Case

The third test case demonstrates the capability of the combination of adaptive meshing technique with the finite element method developed. The problem was presented by Smith and Hutton [9] and the computational domain is shown in Figure 16. The velocity field for this case is given by the following expressions,

$$u = 2y(1-x^2) \quad (24)$$

$$v = -2x(1-y^2) \quad (25)$$

The resulting streamlines are shown in Fig. 16. Along the inlet side, the distribution of ϕ is given by,

$$\phi = 1 + \tanh\left[(2x+1)10\right] \quad (26)$$

The adaptive meshing technique starts from creating a relatively uniform mesh as shown in Fig. 17. The figure also shows the predicted result contours. The adaptive mesh and the corresponding results are also shown in Figure 17. For pure convection, the inlet profile should propagate to the outlet section without any diffusion. Figure 18 compares the outlet profiles of the initial and the adaptive mesh with the exact solution. The figure shows the adaptive mesh provides higher solution accuracy as compared to the initial results because small elements are generated automatically in the regions of high solution gradients behavior.

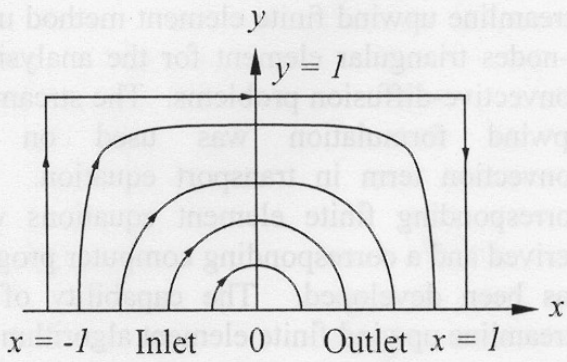

Fig. 16. Smith and Hutton test case.

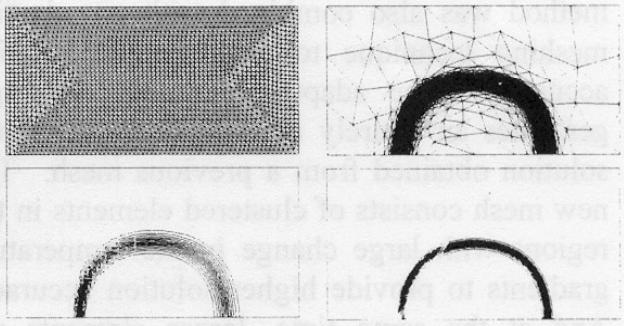

Fig. 17. Initial and final adaptive mesh with its numerical results.

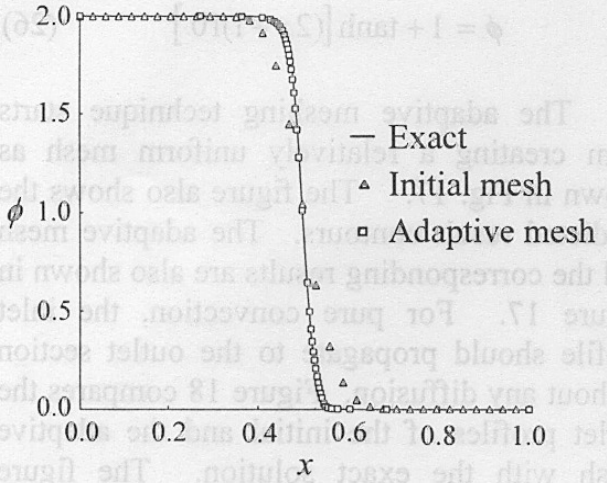

Fig. 18. Comparison of numerical results of the initial and the adaptive mesh along the outflow boundary.

4. Conclusions

This paper presented the adaptive streamline upwind finite element method using 6-nodes triangular element for the analysis of convective-diffusion problems. The streamline upwind formulation was used on the convection term in transport equation. The corresponding finite element equations were derived and a corresponding computer program has been developed. The capability of the streamline upwind finite element algorithm and the corresponding computer program has been evaluated by examples that have prior numerical solutions. The results showed that the current formulation does not exhibit any non-physical spatial oscillation. The current method was also combined with an adaptive meshing technique to improve the solution accuracy. The adaptive meshing technique generates an entirely new mesh based on the solution obtained from a previous mesh. The new mesh consists of clustered elements in the regions with large change in the temperature gradients to provide higher solution accuracy. And at the same time, larger elements are generated in the other regions to reduce the computational time and the computer memory. The combined finite element solution algorithm and the adaptive meshing technique has demonstrated the efficiency of the entire process for improved solution accuracy.

Acknowledgments

The authors are pleased to acknowledge the Thailand Research Fund (TRF) for supporting this research work.

References

[1] Patankar, S.V., (1890). Numerical Heat Transfer and Fluid Flow, Hemisphere, Washington DC.

[2] Brooks, A.N., and Hughes, T.J.R., (1982). Streamline upwind/Petrov-Galerkin for convection dominated flows with particular emphasis on the incompressible Navier-Stokes equations. Comput. Methods Appl. Mech. Eng., Vol.32, pp. 199-259.

[3] Rice, J.G., and Schnipke, R.J., (1984). A monotone streamline upwind finite element method for convection-dominated flows. Comput. Methods Appl. Mech. Eng., Vol.47, pp. 313-327.

[4] Zienkiewicz, O. C., Liu, Y. C., and Huang, G. C., (1989). Error Estimates and Convergence Rates for Various Incompressible Elements. International Journal for Numerical Methods in Engineering, Vol. 28, pp. 2191-2202.

[5] Dechaumphai, P., (1995) "Adaptive Finite Element Technique for Heat Transfer Problems," Journal of Energy, Heat and Mass Transfer, Vol. 17, pp. 87-94.

[6] Dechaumphai, P., (2004). Finite Element Method in Engineering, 3rd Ed., Chulalongkorn University Press, Bangkok.

[7] Fletcher, C.A.J., (1988). Computational Techniques for Fluid Dynamics 1, Springer-Verlag, Berlin.

[8] Brown, G.M., (1960). AIChE Journal, Vol.6, pp. 179-183.

[9] Smith, R.M. and Hutton, T.J.R., (1982) "The numerical treatment of advection: A performance comparison of current methods, Numerical Heat Transfer, Vol.5, pp. 439-461.